Electrodynamics of semiconductor-coated noble metal nanoshells

Jamal T. Manassah*

Department of Electrical Engineering, City College of New York, New York, New York 10031, USA

(Received 28 February 2013; published 29 May 2013)

The full Maxwell equations for a system of concentric shells of a noble metal and a semiconductor, with a very sharp excitonic resonance with a bare frequency in the gap between the bare plasmonic resonant frequency branches and having a strong oscillator strength, are solved. The plasmon-exciton coupling model is verified to produce for this dressed plexcition a spectrum that consists of a splitting of the bare excitonic resonance into two daughters and a shift in the plasmonic resonances from their bare values. The spectral region separating the excitonic daughters exhibits the features characteristic of induced transparency and slow light propagation. Furthermore, I show that the eigenvalues of this coupled system as herein are computed to significantly differ from those obtained in the electrostatic approximation where retardation and radiation reaction terms are neglected.

DOI: 10.1103/PhysRevA.87.053845 PACS number(s): 42.50.Nn, 78.67.−n

I. INTRODUCTION

The problem of plasmon-exciton coupling in different geometric configurations has been addressed recently in a number of publications [1–7]. Within these studies, the feasibility of achieving induced transparency and slow light effects in certain spectral band were examined [8–10].

The goal of identifying a system whereby induced transparency and slow light has been the subject of extensive recent research. Electromagnetically induced transparency (EIT) has been demonstrated for media consisting of metal atoms in the gaseous phase [11], in doped solid-state materials [12], and on quantum-dots-based system [13]. Coupled optical resonators as a classical equivalent to EIT were also recently considered [14]. A system of coupled plasmon-exciton (metal-semiconductor) is one other possible realization of the coupled resonators scheme. The plasmon-exciton coupling observed in this latter case is a direct consequence of imposing the standard continuity equations for the tangential components of the electric field and the magnetic flux density at the different interfaces of the nanostucture.

In this paper I shall examine specifically the detailed full electrodynamics treatment of concentric nanoshells configuration [15–18], but consisting in this case of a noble metal and an inorganic semiconductor. In this instance, the plasmom-exciton coupling controls the dynamics of the system. Furthermore, I shall show that analyzing this problem within the theoretical framework of eigenvalues clarifies the results obtained for the cross sections. The method of eigenvalues is shown, as well, to be a convenient and direct tool for assessing the validity and accuracy of the alternate approximate models.

I shall consider in my analysis a configuration (see Fig. 1) that incorporates as special cases other previously considered cases, specifically, I shall solve for the case of multishells concentric spherical configuration arranged as follows:

dielectric D :	$0 \leqslant r \leqslant \alpha\ R$	region D
noble metal :	$\alpha R \leqslant r \leqslant \beta R$	region C
excitonic material :	$\beta\ R < r \leqslant R$	region B
dielectric A :	$r > R$	region A

Dielectric D is introduced in the model because it is often the case that in a number of standard techniques for preparing spherical nanostructures, it is easiest to start with a seed (typically a silicate), furthermore, varying the radius of the core provides one with the ability to tune the plasmonic resonance to a desired frequency. For simplicity I shall assume here that dielectric D is the vacuum. Dielectric A is the medium in which the ensemble of nanostructure objects are dispersed for ultimate application into a device.

The semiconductor selected should be chosen such that its exciton satisfies the following properties:

(a) A resonance frequency value in the gap separating the two bare plasmonic branches,

(b) a very small spectral width as compared to the noble metal plasmonic spectral line width, and

(c) a large oscillator strength.

As previously pointed out by Yanopapas and Vitanov [19,20] CuCl is a semiconductor which satisfies all of the above properties, if used in conjunction with silver, as the noble metal. I shall use both materials parameters in my illustrations.

Given that the nanosphere that will be considered has mesoscopic dimension ($R \approx 20$ nm), which, while much smaller than the typical optical wavelength, is still much larger than the atomic scale, thus permitting the treatment of each of the active media by classical electrodynamics, and where the different materials in the system are represented by their respective permittivity.

The approach followed here to solve the problem is to start by describing the fields of the E and M modes by the standard solutions of Maxwell equations in spherical geometry, then impose the continuity conditions at the different interfaces and from this set of equations obtain the scattered field. Using the Mie results [21], one can then obtain the scattering and extinction cross sections of the scattered field. In order to interpret the results thus obtained for the spectral distributions, the eigenvalues of the coupled system are obtained. The dependence of these quantities on the geometrical parameters and material parameters are thus obtained.

While in the plasmon hybridization model of a metallic nanoshell, one has, in the dipole approximation, only two modes, the H mode (higher energy mode), which is the antisymmetrically coupled (antibonding) plasmon mode, and

*jmanassah@gmail.com

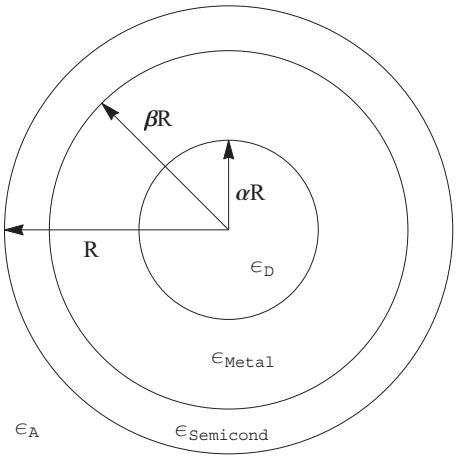

FIG. 1. The geometric configuration of the system considered.

the L mode, which is the symmetrically coupled (bonding) plasmon mode; I show that, in the present configuration, the leading eigenmodes of the system, in the dipole approximation, to consist primarily of four modes, which will be referred to as the "dressed" L mode, two close in frequency modes referred to as the Rl and Rh modes (which are the daughter modes of the original excitonic pole), and the "dressed" H mode. I shall omit henceforth the designation dressed, but these are the modes that are being discussed. Subsequently, I compute the shifts in the plasmonics resonances from their values in the uncoupled case, and find their values for the L mode to be significantly different. Finally, I compute the deviations between the real and imaginary parts of the computed eigenvalues from their values if computed in the approximate electrostatic approximation. The results obtained show that the retardation and radiation reaction terms, which are neglected in the electrostatic approximation, have non-negligible contributions.

It should be noted that all the results given throughout this paper are computed using only the parameters of the particular geometrical configuration and of the constituent equations of the bulk material as previously given. There are no adjustable parameters added.

The paper is organized as follows: In Sec. II the constituent equations for the metal and the semiconductors are given. In Sec. III a review showing the details of obtaining the E and M modes in spherical geometry is given. In Secs. IV and V the details of obtaining the E and M scattered fields for the different partial waves are given. In Sec. VI the lowest order partial-wave contributions to the cross sections are computed. Only the electric dipole mode is found to be significant. In Sec. VII the eigenvalues of the electric dipole mode are computed and directly related to the features observed in Sec. VI. In Sec. VIII the results obtained for the system's eigenvalues, using the full Maxwell equations, are compared with the approximate results obtained using the electrostatic approximation. I conclude in Sec. IX.

II. THE CONSTITUENT EQUATIONS

The relative dielectric of vacuum $\varepsilon_r^{(D)}(\omega)$ is 1, and the immersion medium dielectric is assumed to be constant over the spectral region of interest, I take $\varepsilon_r^{(A)}(\omega) = 1.777$. The permittivity of the excitonic material is taken to be modeled by a single pole Lorentzian [19,20]:

$$\varepsilon_r^{(B)}(\omega) = \varepsilon_{\mathrm{ex},\infty} + f\frac{\gamma}{\omega_0 - \omega - i\gamma}, \tag{1}$$

and the permittivity of the noble metal is taken to be modeled by the Drude approximation as deduced from the Johnson-Christy data [22]:

$$\varepsilon_r^{(C)}(\omega) = \varepsilon_{p,\infty} - \frac{\omega_p^2}{\omega^2 + i\Gamma\omega}. \tag{2}$$

In the figures, except when indicated otherwise, I shall use for illustrative purposes for the values of the above parameters those for CuCl and Ag, namely,

$$\begin{aligned} \varepsilon_{\mathrm{ex},\infty} &= 5.59, \quad f = 632, \quad \hbar\omega_0 = 3.30216\ \mathrm{eV}, \\ \hbar\gamma &= 49.206\ \mu\mathrm{eV}, \quad \varepsilon_{p,\infty} = 3.7, \\ \hbar\omega_p &= 9\ \mathrm{eV}, \quad \hbar\Gamma = 17.28\ \mathrm{meV}. \end{aligned}$$

It should be noted that a more accurate expression [23] than Eq. (2) for the permittivity of silver can be used, if desired, without any further complication in the ensuing treatment.

III. THE ELECTROMAGNETIC MODES IN SPHERICAL GEOMETRY

The sourceless Maxwell equations for fields varying as $\exp(-i\omega t)$are given by

$$\begin{aligned} \vec{\nabla}\circ\vec{B} = 0, \quad \vec{\nabla}\circ\vec{D} = 0, \\ \vec{\nabla}\times\vec{E} - i\omega\vec{B} = 0, \\ \vec{\nabla}\times\vec{H} + i\omega\vec{D} = 0, \end{aligned} \tag{3}$$

with $\vec{H} = \vec{B}/\mu_0$ (no magnetization present) and $\vec{D} = \varepsilon\vec{E}$ (where $\varepsilon = n^2\varepsilon_0$, and n is the index of refraction in each of the separate materials). The quantities ε_0 and μ_0 are related by $c^2 = 1/(\varepsilon_0\mu_0)$, where c is the speed of light in vacuum.

From the above equations, one directly obtains the wave equations

$$\nabla^2\vec{E} + \frac{\omega^2 n^2}{c^2}\vec{E} = 0, \quad \nabla^2 B + \frac{\omega^2 n^2}{c^2}\vec{E} = 0. \tag{4}$$

Solutions of Eqs. (3) and (4) in spherical geometry can be divided into two classes: the electric modes, in which $B_r = 0$, and in magnetic modes, in which $E_r = 0$.

Consider first the electric modes. The magnetic flux density and the electric field are given, for the azimuthally symmetric solutions, by

$$\vec{B} = B_\phi(r,\theta)\hat{e}_\phi, \tag{5}$$

$$\vec{E} = E_r(r,\theta)\hat{e}_r + E_\theta(r,\theta)\hat{e}_\theta. \tag{6}$$

Noting that

$$\vec{\nabla}\times\vec{B} = \frac{1}{r\sin(\theta)}\left\{\frac{\partial}{\partial\theta}[\sin(\theta)B_\phi]\right\}\hat{e}_r - \frac{1}{r}\frac{\partial}{\partial r}(rB_\phi)\hat{e}_\theta \tag{7}$$

and

$$\vec{\nabla}\times\vec{\nabla}\times\vec{B}=\left(-\frac{1}{r}\left[\frac{\partial^2}{\partial r^2}(rB_\phi)\right]-\frac{1}{r}\frac{\partial}{\partial\theta}\left\{\frac{1}{r\sin(\theta)}\frac{\partial}{\partial\theta}[\sin(\theta)B_\phi]\right\}\right)\hat{e}_\phi. \quad (8)$$

Replacing Eq. (8) in the wave equation, one obtains

$$\left[\frac{\partial^2}{\partial r^2}(rB_\phi)\right]+\frac{1}{r^2}\frac{\partial}{\partial\theta}\left\{\frac{1}{\sin(\theta)}\frac{\partial}{\partial\theta}[r\sin(\theta)B_\phi]\right\}+k^2(rB_\phi)=0. \quad (9)$$

Writing the solution as

$$(rB_\phi)=rf(r)\Theta(\theta) \quad (10)$$

and noting that the second term of Eq. (9) can be written as

$$\frac{\partial}{\partial\theta}\left\{\frac{1}{\sin(\theta)}\frac{\partial}{\partial\theta}[r\sin(\theta)B_\phi]\right\}=\frac{1}{\sin(\theta)}\frac{\partial}{\partial\theta}\left[\sin(\theta)\frac{\partial}{\partial\theta}(rB_\phi)\right]-\left[\frac{rB_\phi}{\sin^2(\theta)}\right], \quad (11)$$

the form of $f(r)$ and $\Theta(\theta)$ can be obtained by recalling the differential equations for the associated Legendre polynomials P_l^m and the spherical Bessel functions z_l, namely,

$$\frac{1}{\sin(\theta)}\frac{d}{d\theta}\left\{\sin(\theta)\frac{dP_l^m[\cos(\theta)]}{d\theta}\right\}+\left[l(l+1)-\frac{m^2}{\sin^2(\theta)}\right]P_l^m[\cos(\theta)]=0, \quad (12)$$

$$\frac{d^2z_l(kr)}{dr^2}+\frac{2}{r}\frac{dz_l(kr)}{dr}+\left[k^2-\frac{l(l+1)}{r^2}\right]z_l(kr)=0, \quad (13)$$

then the expression for $B^E_{\phi,l}$, where the superscript E was added to specify that it is for the electric mode, is then given by

$$B^E_{\phi,l}(r,\theta)=z_l(kr)P_l^m[\cos(\theta)]. \quad (14)$$

The corresponding expressions for $E^E_{r,l}(r,\theta)$ and $E^E_{\theta,l}(r,\theta)$ can be obtained using the fourth Maxwell equation, expression (7) for the curl in spherical coordinates, the spherical Bessel functions recursion relation

$$\frac{d}{dy}[yz_l(y)]=yz_{l-1}(y)-lz_l(y), \quad (15)$$

and the expression for the function $G_l(s)$ defined as

$$G_l(s)=\frac{d}{ds}\left[\sqrt{1-s^2}P_l^1(s)\right]=\frac{l}{\sqrt{1-s^2}}\left[sP_l^1(s)-P_{l+1}^1(s)\right]. \quad (16)$$

If one introduces F as the generic symbol for regions (A, B, C, D); and the dimensionless quantities x,u^F defined as $x=r/R$, $u^F=k^FR$ where, as pointed earlier, R is the outer radius of the sphere and k^F is the complex wave number in medium F; the normalized wave vector in each region is given by $u^F=\sqrt{\varepsilon^F(\omega)}\omega R/c$, where $\varepsilon^F(\omega)$ is the permittivity of medium F, and $u_0=\omega R/c$; then the expressions for the azimuthal symmetric magnetic flux density and electric field associated with the E modes are given by

$$\vec{\mathbf{B}}^E_l(x,\theta)=\left[F_l^{(E,1)}j_l(u^Fx)+F_l^{(E,2)}n_l(u^Fx)\right]P_l^1[\cos(\theta)]\hat{e}_\phi=B^E_{\phi,l}(x)P_l^1[\cos(\theta)]\hat{e}_\phi, \quad (17)$$

$$\begin{aligned}\vec{\mathbf{E}}^E(x,\theta)=&-\frac{iu_0}{(u^F)^2x}\left(\left[F_l^{(E,l)}j_l(u^Fx)+F_l^{(E,l)}n_l(u^Fx)\right]\right.\\&\times G_l[\cos(\theta)]\hat{e}_r+\left\{F_l^{(E,l)}[(u^Fx)j_{l-1}(u^Fx)\right.\\&-lj_l(u^Fx)]+F_l^{(E,2)}[(u^Fx)n_{l-1}(u^Fx)\\&\left.\left.-ln_l(u^Fx)]\right\}P_l^1[\cos(\theta)]\hat{e}_\theta\right)\\=&E^E_{r,l}(x)G_l[\cos(\theta)]\hat{e}_r+E^E_{\theta,l}(x)P_l^1[\cos(\theta)]\hat{e}_\theta.\end{aligned} \quad (18)$$

Repeating the above derivations for the M modes, one obtains

$$\vec{\mathbf{E}}^M_l(x,\theta)=\left[F_l^{(M,1)}j_l(u^Fx)+F_l^{(M,2)}n_l(u^Fx)\right]P_l^1[\cos(\theta)]\hat{e}_\phi=E^M_{\phi,l}(x)P_l^1[\cos(\theta)]\hat{e}_\phi, \quad (19)$$

$$\begin{aligned}\vec{\mathbf{B}}^M_l(x,\theta)=&-\frac{i}{u_0x}\left(\left[F_l^{(M,1)}j_l(u^Fx)+F_l^{(M,2)}n_l(u^Fx)\right]\right.\\&\times G_l[\cos(\theta)]\hat{e}_r+\left\{F_l^{(M,1)}[(u^Fx)j_{l-1}(u^Fx)\right.\\&-lj_l(u^Fx)]+F_l^{(M,2)}[(u^Fx)n_{l-1}(u^Fx)\\&\left.\left.-ln_l(u^Fx)]\right\}P_l^1[\cos(\theta)]\hat{e}_\theta\right)\\=&B^M_{r,l}(x)G_l[\cos(\theta)]\hat{e}_r+B^M_{\theta,l}(x)P_l^1[\cos(\theta)]\hat{e}_\theta.\end{aligned} \quad (20)$$

Obtaining the different physical quantities associated with the scattered field starts with determining the values of the respective F for a given incoming field.

IV. THE E-MODES SOLUTIONS

In order to find the different values of the F_l for the physical problem of an incoming plane wave propagating in the z direction, one needs to use the partial-wave expansion of $\exp(ikz)$, namely,

$$\exp(ikz)=\sum_{l=0}^{\infty}(i)^l(2l+1)j_l(kr)P_l[\cos(\theta)]. \quad (21)$$

The E-modes solutions in the different regions of the sphere are given by adding the expression of the scattered field obtained in Sec. III to that of the incoming field and requiring that the tangential components of the electric field and the magnetic flux density be continuous at each of the interfaces. The magnetic flux density in the different regions is given by

$$\begin{aligned}\mathbf{B}^E_{\phi,l}&=D_l^{(E,1)}j_l(u^Dx), && 0\leqslant r\leqslant\alpha R,\\ \mathbf{B}^E_{\phi,l}&=C_l^{(E,1)}j_l(u^Cx)+C_l^{(E,2)}n_l(u^Cx), && \alpha R<r\leqslant\beta R,\\ \mathbf{B}^E_{\phi,l}&=B_l^{(E,1)}j_l(u^Bx)+B_l^{(E,2)}n_l(u^Bx), && \beta R<r\leqslant R,\\ \mathbf{B}^E_{\phi,l}&=j_l(u^Ax)+A_l^Eh_l^{(1)}(u^Ax), && r>R.\end{aligned} \quad (22)$$

The different functional forms in the different regions of space arise from the requirements that the solution be finite at the origin, and that the scattered field be outgoing outside the

nanosphere. The continuity of $\mathbf{B}_\phi$ at $x=\alpha$, $x=\beta$, and $x=1$ (the materials are assumed to have no internal magnetization) gives the equations

$$D_l^{(E,1)} j_l(u^D\alpha) = C_l^{(E,1)} j_l(u^C\alpha) + C_l^{(E,2)} n_l(u^C\alpha), \quad (23)$$

$$C_l^{(E,1)} j_l(u^C\beta) + C_l^{(E,2)} n_l(u^C\beta) = B_l^{(E,1)} j_l(u^B\beta) + B_l^{(E,2)} n_l(u^B\beta), \quad (24)$$

$$B_l^{(E,1)} j_l(u^B) + B_l^{(E,2)} n_l(u^B) = j_l(u^A) + A_l^{(E)} h_1^{(1)}(u^A). \quad (25)$$

The continuity of $\mathbf{E}_\theta$ at $x=\alpha$, $x=\beta$, $x=1$, gives the set of equations

$$\begin{aligned} &D_l^{(E,1)}(u^C)^2[u^D\alpha j_{l-1}(\alpha u^D) - l j_l(\alpha u^D)] \\ &\quad = C_l^{(E,1)}(u^D)^2[u^C\alpha j_{l-1}(\alpha u^C) - l j_l(\alpha u^C)] \\ &\qquad + C_l^{(E,2)}(u^D)^2[u^C\alpha n_{l-1}(\alpha u^C) - l n_l(\alpha u^C)], \end{aligned} \quad (26)$$

$$\begin{aligned} &C_l^{(E,1)}(u^B)^2[u^C\beta j_{l-1}(\beta u^C) - l j_l(\beta u^C)] \\ &\qquad + C_l^{(E,2)}(u^B)^2[u^C\beta n_{l-1}(\beta u^C) - l n_l(\beta u^C)] \\ &\quad = B_l^{(E,1)}(u^C)^2[u^B\beta j_{l-1}(\beta u^B) - l j_l(\beta u^B)] \\ &\qquad + B_l^{(E,2)}(u^C)^2[u^B\beta n_{l-1}(\beta u^B) - l n_l(\beta u^B)], \end{aligned} \quad (27)$$

$$\begin{aligned} &B_l^{(E,1)}(u^A)^2[u^B j_{l-1}(u^B) - l j_l(u^B)] \\ &\qquad + B_l^{(E,2)}(u^A)^2[u^B n_{l-1}(u^B) - l n_l(u^B)] \\ &\quad = (u^B)^2[u^A j_{l-1}(u^A) - l j_l(u^A)] \\ &\qquad + A_l^{(E)}(u^B)^2\left[u^A h_{l-1}^{(1)}(u^A) - l h_1^{(1)}(u^A)\right]. \end{aligned} \quad (28)$$

In Eqs. (23) and (26), $h_l^{(1)} = j_l + i n_l$.

Equations (21)–(26) can be written in the matrix form:

$$\left[\mathbf{M}_l^E\right] \begin{pmatrix} D_l^{(E,1)} \\ C_l^{(E,1)} \\ C_l^{(E,2)} \\ B_l^{(E,1)} \\ B_l^{(E,2)} \\ A_l^{(E)} \end{pmatrix} = \begin{pmatrix} 0 \\ 0 \\ 0 \\ 0 \\ j_l(u^A) \\ (u^B)^2 j_{V,l}(u^A) \end{pmatrix}, \quad (29)$$

where the matrix $\mathbf{M}_l^E$ is given by

$$\left[\mathbf{M}_l^E\right] = \begin{pmatrix} j_l(\alpha u^D) & -j_l(\alpha u^C) & -n_l(\alpha u^C) & 0 & 0 & 0 \\ (u^C)^2 j_{V,l}(\alpha u^D) & -(u^D)^2 j_{V,l}(\alpha u^C) & -(u^D)^2 n_{V,l}(\alpha u^C) & 0 & 0 & 0 \\ 0 & j_l(\beta u^C) & n_l(\beta u^C) & -j_l(\beta u^B) & -n_l(\beta u^B) & 0 \\ 0 & (u^B)^2 j_{V,l}(\beta u^C) & (u^B)^2 n_{V,l}(\beta u^C) & -(u^C)^2 j_{V,l}(\beta u^B) & -(u^C)^2 n_{V,l}(\beta u^B) & 0 \\ 0 & 0 & 0 & j_l(u^B) & n_l(u^B) & -h_l^{(1)}(u^A) \\ 0 & 0 & 0 & (u^A)^2 j_{V,l}(u^B) & (u^A)^2 n_{V,l}(u^B) & -(u^B)^2 h_{V,l}^{(1)}(u^A) \end{pmatrix}, \quad (30)$$

$$j_{V,l}(w) = w j_{l-1}(w) - l j_l(w),\ n_{V,l}(w) = w n_{l-1}(w) - l n_l(w), \text{ and } h_{V,l}^{(1)}(w) = w h_{l-1}^{(1)}(w) - l h_l^{(1)}(w).$$

V. THE *M*-MODES SOLUTIONS

The solutions for the M modes can be obtained as well by using the boundary conditions for the tangential components of the electric fields and the magnetic flux density, giving

$$\left[\mathbf{M}_l^M\right] = \begin{pmatrix} D_l^{(M,1)} \\ C_l^{(M,1)} \\ C_l^{(M,2)} \\ B_l^{(M,1)} \\ B_l^{(M,2)} \\ A_l^{(M)} \end{pmatrix} = \begin{pmatrix} 0 \\ 0 \\ 0 \\ 0 \\ j_l(u^A) \\ j_{V,l}(u^A) \end{pmatrix}, \quad (31)$$

where the matrix $\mathbf{M}_l^M$ is given by

$$\left[\mathbf{M}_l^M\right] = \begin{pmatrix} j_l(\alpha u^D) & -j_l(\alpha u^C) & -n_l(\alpha u^C) & 0 & 0 & 0 \\ j_{V,l}(\alpha u^D) & -j_{V,l}(\alpha u^C) & -n_{V,l}(\alpha u^C) & 0 & 0 & 0 \\ 0 & j_l(\beta u^C) & n_l(\beta u^C) & -j_l(\beta u^B) & -n_l(\beta u^B) & 0 \\ 0 & j_{V,l}(\beta u^C) & n_{V,l}(\beta u^C) & -j_{V,l}(\beta u^B) & -n_{V,l}(\beta u^B) & 0 \\ 0 & 0 & 0 & j_l(u^B) & n_l(u^B) & -h_l^{(1)}(u^A) \\ 0 & 0 & 0 & j_{V,l}(u^B) & n_{V,l}(u^B) & -h_{V,l}^{(1)}(u^A) \end{pmatrix}, \quad (32)$$

and all the parameters are as previously defined.

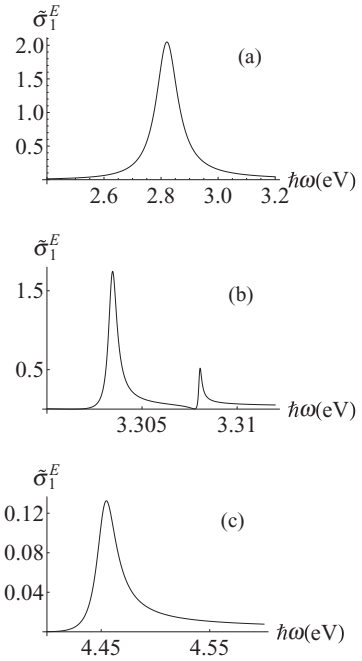

FIG. 2. The electric dipole contribution to the normalized scattering cross section is plotted as function of the incoming frequency in the different spectral windows. (a) The L window; (b) the Rl-Rh window; and (c) the H window. $R = 20$ nm, $\alpha = 0.5$, $\beta = 0.95$.

VI. THE SCATTERING AND THE EXTINCTION CROSS SECTIONS

All the information about the scattered field is contained in the expressions of $\{A_l^E\}$ and $\{A_l^B\}$. Mie's theory [21] showed that the scattering cross section (i.e., the power scattered divided by the incident flux) and the extinction cross section (i.e., the sum of the scattering and absorption cross sections) can be written as sums of independent multipole contributions, namely,

$$\sigma_{\text{scat.}} = \frac{2\pi}{(k^A)^2}\sum_{l=1}^{\infty}(2l+1)\left(\left|A_l^E\right|^2+\left|A_l^M\right|^2\right) = \frac{2\pi}{(k^A)^2}\sum_{l=1}^{\infty}\left(\tilde{\sigma}_l^E+\tilde{\sigma}_l^M\right) \tag{33}$$

and

$$\sigma_{\text{ext}} = \frac{2\pi}{(k^A)^2}\sum_{l=1}^{\infty}(2l+1)\text{Re}\left(A_l^E+A_l^M\right) = \frac{2\pi}{(k^A)^2}\sum_{l=1}^{\infty}\text{Re}\left(\tilde{A}_l^E+\tilde{A}_l^M\right). \tag{34}$$

The contributions of the different partial modes can be investigated by plotting the lowest order modes components of the total scattering. I plot in Fig. 2 a function of the incoming frequency, the electric dipole contribution in the three windows where this quantity has maxima. I shall refer hereafter to the mode showing in Fig. 2(a) as the L mode (L is for the dressed lower frequency branch of the plasmonic resonance spectrum), the two dressed excitonic daughter modes appearing in Fig. 2(b) as the Rl and Rh modes (R for the excitonic resonance, and l and h, respectively, for lower and higher branches), and the mode showing in Fig. 2(c) as the H mode (H for the dressed higher branch of the plasmonic resonance spectrum). The two most prominent features of these figures are that:

(a) the excitonic resonance has split into two daughter peaks instead of the single excitonic peak present in the isolated semiconductor; and

(b) the peaks of the dressed plasmonics resonances have shifted from their isolated metal or bare values.

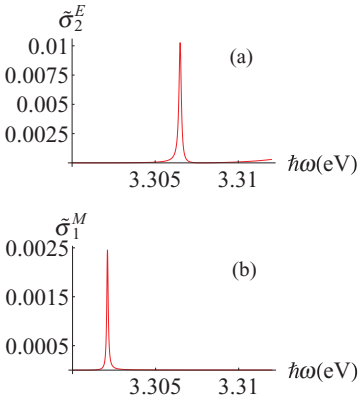

FIG. 3. (Color online) (a) The electric quadrupole and (b) the magnetic dipole contributions to the normalized scattering cross section are plotted as function of the incoming field's frequency in the Rl-Rh spectral window. $R = 20$ nm, $\alpha = 0.5$, $\beta = 0.95$.

In Fig. 3 I plot as a function of the incoming frequency, respectively, the contributions of the electric quadrupole and magnetic dipole to the scattering cross section in the same spectral window as that of Fig. 2(b). As can be observed, the contribution from either modes is negligible in the region of interest for induced transparency and slow light, i.e., in between the maxima of the Rl and Rh modes. Given the minor contributions of all other modes than the electric dipole mode to the scattering cross section, for the considered nanostructure ($R \approx 20$ nm) I shall henceforth restrict my analysis to the electric dipole mode.

In Fig. 4 I plot the real part and imaginary parts of A_1^E in the spectral window of Fig. 2(b), the real part gives essentially the

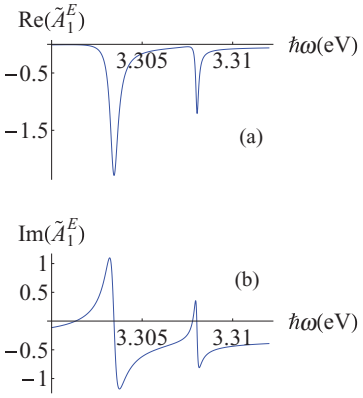

FIG. 4. (Color online) (a) Re($\tilde{A}_1^E$) and (b) Im($\tilde{A}_1^E$) are plotted as function of the incoming frequency in the Rl-Rh spectral window. $R = 20$ nm, $\alpha = 0.5$, $\beta = 0.95$.

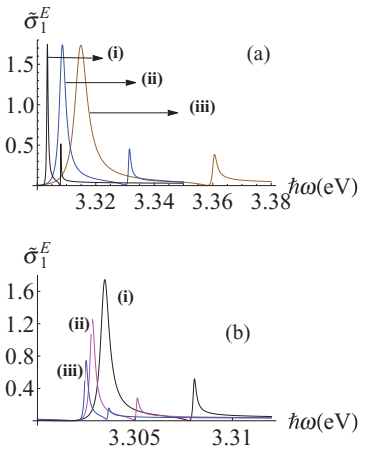

FIG. 5. (Color online) The electric dipole contribution to the normalized scattering cross section is plotted as function of the incoming frequency in the *Rl*-*Rh* window, for different values of one of the excitonic parameters. (a) (i) $\gamma = \gamma_{\mathrm{CuCl}}$, (ii) $\gamma = 5\gamma_{\mathrm{CuCl}}$, (iii) $\gamma = 10\gamma_{\mathrm{CuCl}}$. The values of f and ω_0 are kept fixed and equal to those of CuCl. (b) (i) $f = f_{\mathrm{CuCl}}$, (ii) $f = \frac{1}{2} f_{\mathrm{CuCl}}$, (iii) $f = \frac{1}{4} f_{\mathrm{CuCl}}$. γ and ω_0 are those of CuCl. Everywhere: $R = 20\,\mathrm{nm}$, $\alpha = 0.5$, $\beta = 0.95$

extinction coefficient for the incoming wave in that window (note the dip there, indicating very low absorption), and the imaginary part shows the strong dispersion associated with the slowing of the light. (I shall examine elsewhere the details of the method to optimize the system configurations to tailor these effects to specific applications.)

In Fig. 5 I plot the scattering cross section in the *Rl*-*Rh* region, if one were to change arbitrarily the values of either the excitonic damping constant [Fig. 5(a)] or the oscillator strength [Fig. 5(b)] in the excitonic permittivity.

As can be observed, the positions of the maxima of the *Rl* and *Rh* modes, their width and their interseparation are very sensitive to the values of these two intrinsic excitonic parameters. These figures also indicate the range of values for which the desired topology in the *Rl*-*Rh* spectral distribution is preserved.

VII. THE EIGENMODES ANALYSIS

In the preceding section I kept referring qualitatively to certain eigenmodes but did not give a rigorous meaning to these quantities. In this section I shall provide a more rigorous definition to those quantities, and find a more suggestive way to express them.

As pointed out in Secs. IV and V, both A_l^E and A_l^M are obtained by first inverting, respectively, the matrices $\mathbf{M}_l^E$ and $\mathbf{M}_l^M$. This means that

$$A_l^E(\omega) = \frac{N_l^E(\omega)}{\Delta_l^E(\omega)}, \tag{35}$$

with a similar expression for A_l^M. The numerator of Eq. (35) is the sum of cofactors of the matrix $\mathbf{M}_l^E$ and of the incoming fields spherical expansion coefficients. The denominator in Eq. (35) is uniquely determined by the geometry and the material used in the different regions of the system and is always given by

$$\Delta_l^E(\omega) = \det\left[\mathbf{M}_l^E(\omega)\right]. \tag{36}$$

Now consider an expression of the form

$$f(u) = \frac{N(u)}{(u-\omega)\,\Delta(u)}, \tag{37}$$

and assume that the function $\mathrm{N}(u)/\Delta(u)$ is meromorphic in the complex u plane, $\Delta(u)$ has simple zeros at $\hat{\omega}_n$, $n = 1,2,3,\ldots$, and ω is different from any of these zeros; then the poles of $f(u)$ are all simple and located at the zeros of $\Delta(u)$ and at ω. Now consider a contour at infinity C_∞, the residue theorem allows one to write

$$\frac{1}{2\pi i}\oint_{C_\infty} \frac{N(u)}{\Delta(u)\,(u-\omega)}du = \frac{N(\omega)}{\Delta(\omega)} + \sum_{n=1}^{\infty} \frac{N\left(\hat{\omega}_n\right)}{\Delta'\left(\hat{\omega}_n\right)\left(\hat{\omega}_n - \omega\right)}. \tag{38}$$

The contour integral vanishes if $\lim_{u\to\infty} \frac{N(u)}{\Delta(u)} = 0$, and consequently the ratio $N(\omega)/\Delta(\omega)$ can be written in the alternative form:

$$\frac{N(\omega)}{\Delta(\omega)} = \sum_{n=1}^{\infty} \frac{N\left(\hat{\omega}_n\right)}{\Delta'\left(\hat{\omega}_n\right)\left(\omega - \hat{\omega}_n\right)}. \tag{39}$$

This expression is known as the Mittag-Leffler expansion, where $\{\hat{\omega}_n\}$ are the complex roots of any of the expressions $\det(\mathbf{M}_l^E) = 0$, or $\det(\mathbf{M}_l^M) = 0$, as the case may be.

The above result leads us to the conclusion that if a plot of the function $|A_l^E(\omega)|$ or $|A_l^M(\omega)|$ has n maxima, then this indicates that $\Delta(\omega)$ has n roots in the complex plane, and that Eq. (39) is an alternative way to writing this quantity. Thus, finding the zeros of the determinant of the matrices $\mathbf{M}_l^E$ and $\mathbf{M}_l^M$, also called the eigenvalues of the system, takes special importance. The real part of any of these eigenvalues corresponds to the value of ω at the corresponding maximum in the total cross section and its imaginary part approximates the width of this maximum.

In Figs. 6 and 7 I plot the real and imaginary parts of the different eigenvalues that were denoted by the symbols (*L*, *Rl*,

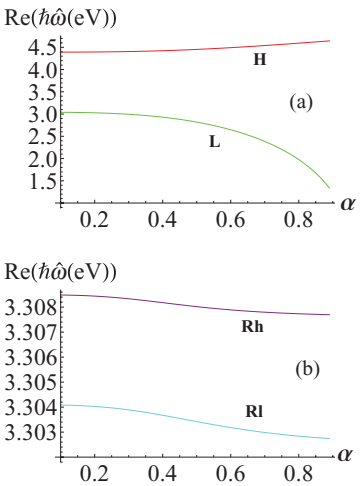

FIG. 6. (Color online) The real part of all the eigenvalues $\mathrm{Re}(\hat{\omega})$ are plotted as function of the normalized core radius. (a) The *L* and *H* modes. (b) The *Rl* and *Rh* modes. $R = 20\,\mathrm{nm}$, $\beta = 0.95$.

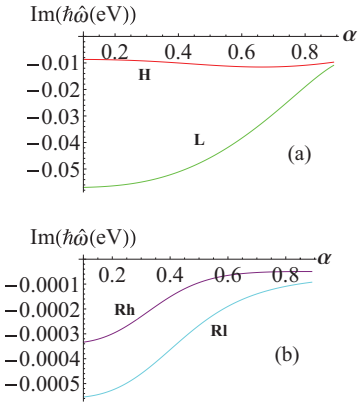

FIG. 7. (Color online) The imaginary part of the eigenvalues $\mathrm{Im}(\hat{\omega})$ are plotted as a function of the normalized core radius. (a) The L and H modes. (b) The Rl and Rh modes. $R = 20$ nm, $\beta = 0.95$.

Rh, H) as function of α [where the thickness of the noble metal shell is $(\beta - \alpha)R$] for a fixed value of the semiconductor shell [the interval $(\beta R, R)$]. Note that the separation in the resonance frequency of the daughters is everywhere much larger than the resonances width, thus confirming the required condition for obtaining low absorption, slowing of light in the spectral region separating the two excitonic daughters.

Of particular interest, note

(i) the dressed L resonance can be tuned to any frequency in a window extending all the way from the violet to the near infra-red; and

(ii) the 1 to 2 order of magnitude increase in the width of the dressed excitonic lines from their bare values—a common feature observed when comparing the imaginary part of the eigenvalues of a coupled system with those of the diagonal elements (bare values).

In Figs. 8 and 9 I plot the modifications to the real and imaginary values of the dressed plasmonics resonances from

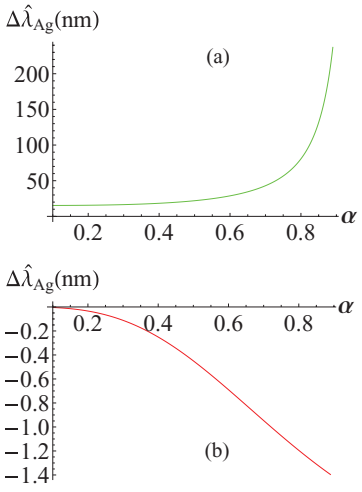

FIG. 8. (Color online) The shift in the dressed ($\beta = 0.95$) plasmonic resonance wavelength from its bare value ($\beta = 1$) as a function of the normalized core radius. $R = 20$ nm. (a) L mode and (b) H mode.

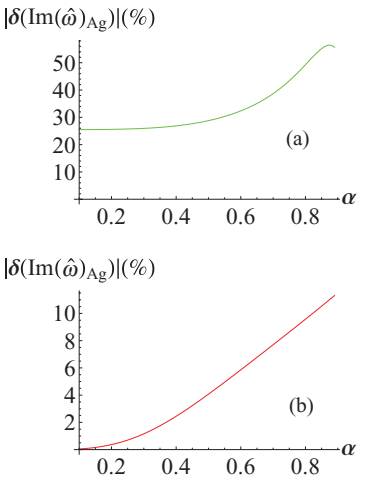

FIG. 9. (Color online) The relative change in the imaginary part of the plasmonic eigenvalue of the dressed case ($\beta = 0.95$) and its bare value ($\beta = 1$) is plotted as function of the normalized core radius. $R = 20$ nm. (a) L mode and (b) H mode.

their bare values. The quantities plotted are, respectively,

$$\Delta\hat{\lambda}_{\mathrm{Ag}} = \hat{\lambda}_{\mathrm{dressed}} - \hat{\lambda}_{\mathrm{bare}}, \tag{40}$$

$$\delta(\mathrm{Im}(\hat{\omega})_{\mathrm{Ag}}) = \left| \frac{\mathrm{Im}\,(\hat{\omega}_{\mathrm{dressed}}) - \mathrm{Im}\,(\hat{\omega}_{\mathrm{bare}})}{\mathrm{Im}\,(\hat{\omega}_{\mathrm{dressed}})} \right| \times 100. \tag{41}$$

One observes that both the wavelength and the width of both dressed plasmonic resonances for the coupled system are substantially different from their values for the case that $\beta = 1$ (i.e., no semiconductor is present). The closeness of the excitonic resonance to the L-plasmonic branch impacts the later more substantially than it does the H branch, and leads to a larger shift in the resonances wavelength, and a large deviation in the linewidth. [Compare, respectively, Figs. 8(a), 8(b) and Figs. 9(a), 9(b)].

VIII. ELECTROSTATIC MODEL

Given that the electrostatic approximation to Maxwell equations have often been used in analyzing nanostructures, I shall next compute the eigenvalues for the present configuration in this approximation and compare the obtained results with those deduced earlier in this paper using the full Maxwell equations. But before embarking on the mathematical details of the electrostatic approximation solution, let us pause and recall what constitutes the difference between the full and approximate theories, at the atomic level.

In the electrostatic approximation, the interaction of two dipoles is the instantaneous short-range r^{-3} dipole-dipole interaction; while in the full theory, the interaction between two dipoles is given by the Lienard-Wiechert potential. This potential has in addition to the short term component also long range r^{-1},r^{-2} terms, consequently introducing size dependence, referred to as retardation effects when considering a finite size sphere. This potential also includes an imaginary part, the so-called radiation damping terms. These terms substantially modify the linewidth of the resonances in addition to that of the intrinsic value.

I shall now give the details for deriving the eigenvalues in the electric approximation. In the electrostatic approximation, the electric field obeys the equations

$$\vec{E} = -\vec{\nabla} V, \tag{42}$$

$$\vec{\nabla} \circ (\varepsilon \vec{E}) = 0. \tag{43}$$

For spherical geometry Eqs. (42) and (43) lead in the dipole approximation to the following form of the electric potential in the different regions:

$$V(r,\theta) = \begin{cases} \mathcal{D}^{(1)} r \cos(\theta), & 0 \leqslant r \leqslant \alpha R, \\ \left(\mathcal{C}^{(1)} r + \mathcal{C}^{(2)} \frac{R^3}{r^2}\right) \cos(\theta), & \alpha R \leqslant r \leqslant \beta R, \\ \left(\mathcal{B}^{(1)} r + \mathcal{B}^{(2)} \frac{R^3}{r^2}\right) \cos(\theta), & \beta R \leqslant r \leqslant R, \\ \mathcal{A}^{(2)} \frac{R^3}{r^2} \cos(\theta), & r > R. \end{cases} \tag{44}$$

The terms proportional respectively to (r^{-2}, r) in the regions enclosing $(r = 0, r = \infty)$ were set equal to zero to ensure that the expression for the potential is everywhere finite.

The continuity of V at the different interfaces requires that

$$\mathcal{A}^{(2)} = \mathcal{B}^{(1)} + \mathcal{B}^{(2)}, \tag{45}$$

$$\beta^3 \mathcal{B}^{(1)} + \mathcal{B}^{(2)} = \beta^3 \mathcal{C}^{(1)} + \mathcal{C}^{(2)}, \tag{46}$$

$$\alpha^3 \mathcal{C}^{(1)} + \mathcal{C}^{(2)} = \alpha^3 \mathcal{D}^{(1)}. \tag{47}$$

The continuity of $(\varepsilon \partial V/\partial r)$at the different interfaces requires that

$$-2\varepsilon^{(A)} \mathcal{A}^{(2)} = (\mathcal{B}^{(1)} - 2\mathcal{B}^{(2)}), \tag{48}$$

$$\varepsilon^{(B)} (\beta^3 \mathcal{B}^{(1)} - 2\mathcal{B}^{(2)}) = \varepsilon^{(C)} (\beta^3 \mathcal{C}^{(1)} - 2\mathcal{C}^{(2)}), \tag{49}$$

$$\varepsilon^{(C)} (\alpha^3 \mathcal{C}^{(1)} - 2\mathcal{C}^{(2)}) = \varepsilon^{(D)} \alpha^3 \mathcal{D}^{(1)}. \tag{50}$$

The eigenvalues in the electrostatic approximation for the dipole mode will be the roots of the equationdet$(\mathbf{M}^{\text{Stat}}_{l=1}) = 0$, where

$$\mathbf{M}^{\text{Stat}}_{l=1} = \begin{pmatrix} 1 & -1 & -1 & 0 & 0 & 0 \\ 0 & \beta^3 & 1 & -\beta^3 & -1 & 0 \\ 0 & 0 & 0 & \alpha^3 & 1 & -\alpha^3 \\ -2\varepsilon^{(A)} & -\varepsilon^{(B)} & +2\varepsilon^{(B)} & 0 & 0 & 0 \\ 0 & \varepsilon^{(B)}\beta^3 & -2\varepsilon^{(B)} & -\varepsilon^{(C)}\beta^3 & +2\varepsilon^{(C)} & 0 \\ 0 & 0 & 0 & \varepsilon^{(C)}\alpha^3 & -2\varepsilon^{(C)} & -\varepsilon^{(D)}\alpha^3 \end{pmatrix}. \tag{51}$$

In Figs. 10 and 11 I plot the deviations of the real and imaginary parts of the dressed plasmonics eigenvalues in the electrostatic approximation from their Maxwell values.

The quantities plotted are defined as follows:

$$\Delta\hat{\lambda}_{\text{Stat}} = \hat{\lambda} - \hat{\lambda}_{\text{Stat}}, \tag{52}$$

$$\delta(\text{Im}\,(\hat{\omega})_{\text{Stat}}) = \left| \frac{\text{Im}\,(\hat{\omega}) - \text{Im}\,(\hat{\omega}_{\text{Stat}})}{\text{Im}\,(\hat{\omega})} \right| \times 100. \tag{53}$$

The subscript Stat is used to identify the quantities computed in the electrostatic approximation.

One notes that although the radius of the sphere is only 20 nm, the deviations in the values of both the real and imaginary parts of the eigenvalues can be substantial; thus leading to the conclusion that the errors in the electrostatic approximation exceed the experimental accuracy with which the resonance frequencies and widths can be measured.

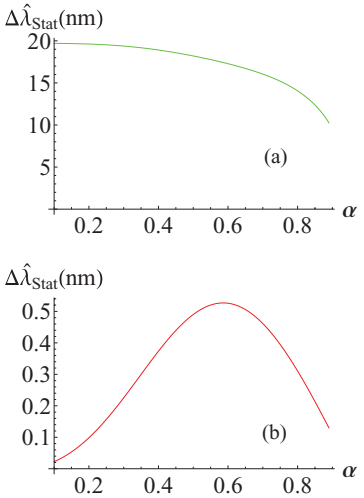

FIG. 10. (Color online) The shift in the dressed resonance plasmonic wavelengths from their approximate electrostatic values is plotted as function of the normalized core radius. $R = 20$ nm. $\beta = 0.95$. (a) L mode and (b) H mode.

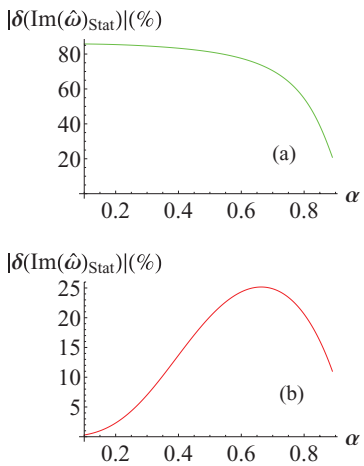

FIG. 11. (Color online) The relative change in the imaginary part of the plasmonic eigenvalues of the dressed case and their approximate electrostatic values is plotted as function of the normalized core radius. $R = 20$ nm. $\beta = 0.95$. (a) L mode and (b) H mode.

IX. CONCLUSION

In this paper I examined a system of concentric shells consisting of a noble metal and a semiconductor, with a very sharp excitonic resonance with a bare frequency in the gap between the bare plasmonic resonant frequency branches and having a strong oscillator strength. The plasmon-exciton coupling leads to the following physical results:

(i) A splitting of the excitonic line occurs. The spectral region separating the excitonic daughters satisfies the conditions for induced transparency and slow light propagation.

(ii) The plasmonics resonances, especially the L mode, are shifted from their bare values.

Quantitatively I show that the full-Maxwell results obtained differ markedly from those of the electrostatic model. Furthermore, I show that the maxima observed in the partial cross-section results obtained for the dipolar mode can be identified with the complex zeros of the scattering matrix characteristic determinant.

Finally, it is worth pointing out that the above analysis provides yet another successful application of the eigenvalue technique to probe the physical properties of concentric nanoshells. Friedberg and the author formulated this technique first in [24,25] while investigating the cooperative decay rate and cooperative Lamb shift of an ensemble of resonant atoms in a small sphere. This technique was subsequently used, as well, in analyzing the deviation from Dicke's results for the superradiant rate in a small sphere with radially dependent density [26,27]; in computing the plasmonic resonances in a metallic nanoshell [28] and in multiple metallic shells [29]; and in predicting and analyzing the Purcell-Dicke superradiant-enhancing effect [30,31].

On the practical side, optimizing the above system parameters has the potential of identifying designs for ultrasensitive laser-based gyroscopes and gravity/general relativity effects detecting instrumentations [32,33], the details of this optimization will be reported elsewhere.

[1] A. O. Govorov, G. W. Bryant, N. Zhang, T. Skeini, J. Lee, N. A. Kotov, J. M. Slocik, and R. R. Naik, Nano Lett. **6**, 984 (2006).

[2] W. Zhang, A. O. Govorov, and G. W. Bryant, Phys. Rev. Lett. **97**, 146804 (2006).

[3] R. D. Artuso and G. W. Bryant, Nano Lett. **8**, 2106 (2008).

[4] N. T. Fofang, T. H. Park, O. Neumann, N. A. Mirin, P. Nordlander, and N. J. Halas, Nano Lett. **8**, 3481 (2008).

[5] S. M. Sadeghi, L. Deng, X. Li, and W. P. Huang, Nanotechnology **20**, 365401 (2009).

[6] A. Manjavacas, F. J. Garcia de Abajo, and P. Nordlander, Nano Lett. **11**, 2318 (2011).

[7] A. Panahpour, Y. Silani, M. Farrokhian, A. Lavrinenko, and H. Latifi, J. Opt. Soc. Am. B **209**, 2297 (2012).

[8] P. Tassin, L. Zhang, Th. Koschny, E. N. Economou, and C. M. Soukoulis, Phys. Rev. Lett. **102**, 053901 (2009).

[9] R. D. Kekatpure, E. S. Barnard, W. Cai, and M. L. Brongersma, Phys. Rev. Lett. **104**, 243902 (2010).

[10] X. Wu, S. K. Gray, and M. Pelton, Opt. Express **18**, 2363 (2010).

[11] See the review article: M. Fleishhauer, A. Imamoglu, and J. P. Marangos, Rev. Mod. Phys. **77**, 633 (2005).

[12] B. S. Ham, M. S. Shahriar, M. K. Kim, and P. R. Hemmer, Opt. Lett. **22**, 1849 (1997).

[13] S. Marcinkevicuis, A. Gusheterov, and J. P. Reithmayer, Appl. Phys. Lett. **92**, 041113 (2008).

[14] Q. Xu, S. Sandhu, M. L. Povinelli, J. Shakya, S. Fan, and M. Lipson, Phys. Rev. Lett. **96**, 123901 (2006).

[15] R. Paniagua-Dominguez, F. Lopez-Tejiara, R. Marques, and J. A. Sanchez-Gil, New J. Phys. **13**, 123017 (2011).

[16] W. Liu, A. E. Miroshnichenko, D. N. Neshev, and Y. S. Kivshar, ACS Nano **6**, 5489 (2012).

[17] W. Liu, A. E. Miroshnichenko, D. N. Neshev, and Y. S. Kivshar, Phys. Rev. B **86**, 081407(R) (2012).

[18] D. J. Wu, S. M. Jiang, Y. Cheng, and X. J. Liu, Opt. Express **21**, 1076 (2013).

[19] V. Yannopapas and N. V. Vitanov, Phys. Rev. B **74**, 193304 (2006).

[20] V. Yannopapas, Phys. Status Solidi B **245**, 992 (2008).

[21] G. Mie, Ann. Phys. (Leipzig) **25**, 377 (1908); See also the textbook C. F. Bohren and D. R. Huffman, *Absorption and Scattering of Light by Small Particles* (Wiley, New York, 1983).

[22] P. B. Johnson and R. W. Christy, Phys. Rev. B **6**, 4370 (1972).

[23] V. P. Drashev, U. K. Chettiar, A. Kildishev, H. K. Yuan, W. Cai, and V. M. Shalaev, Opt. Express **16**, 1186 (2008).

[24] R. Friedberg and J. T. Manassah, Phys. Lett. A **372**, 6833 (2008).

[25] R. Friedberg and J. T. Manassah, Phys. Lett. A **373**, 4416 (2009).

[26] R. Friedberg and J. T. Manassah, Phys. Rev. A **85**, 013834 (2012).

[27] R. Friedberg and J. T. Manassah, Phys. Rev. A **85**, 033834 (2012).

[28] R. Friedberg and J. T. Manassah, Chem. Phys. Lett. **539–540**, 118 (2012).

[29] J. T. Manassah, Phys. Lett. A **376**, 2600 (2012).

[30] J. T. Manassah, Laser Phys. **22**, 738 (2012).

[31] R. Friedberg and J. T. Manassah, Phys. Rev. A **86**, 023804 (2012).

[32] M. O. Scully, M. S. Zubairy, and K. Just, Phys. Lett. A **77**, 88 (1980).

[33] J. T. Manassah, Phys. Lett. A **113**, 151 (1985).